Multi-scale Aspects of Convective Systems Associated with an Intraseasonal Oscillation over the Indonesian Maritime Continent

Yoshiaki SHIBAGAKI,

Faculty of Information and Communication Engineering,

Osaka Electro-Communication University, Osaka, Japan,

Toyoshi SHIMOMAI, Toshiaki KOZU,

Interdisciplinary Faculty of Science and Engineering, Shimane University,

Shimane, Japan,

Shuichi MORI,

Institute of Observational Research System for Global Change

Japan Agency for Marine-Earth Science and Technology, Yokohama, Japan

Yasushi FUJIYOSHI[*],

Institute of Low Temperature Science, Hokkaido University, Sapporo, Japan

Hiroyuki HASHIGUCHI, Masayuki K. YAMAMOTO, Shoichiro FUKAO,

Research Institute for Sustainable Humanosphere, Kyoto University, Kyoto, Japan,

and

Manabu D. YAMANAKA[**]

Graduate School of Science and Technology, Kobe University, Kobe Japan

* Additional affiliation: Frontier Research Center for Global Change,

  Japan Agency for Marine-Earth Science and Technology, Yokohama, Japan

** Additional affiliation: Institute of Observational Research System for Global Change,

  Japan Agency for Marine-Earth Science and Technology, Yokohama, Japan

*Corresponding author:

 Yoshiaki Shibagaki, Osaka Electro-Communication University,

 18-8 Hatsu-cho, Neyagawa, Osaka 572-8530, Japan

 E-mail: sibagaki@maelab.osakac.ac.jp

Abstract

Multi-scale aspects of convective systems over the Indonesian maritime continent in the convectively active phase of an intraseasonal oscillation (ISO) during November 2002 are studied, using Geostationary Meteorological Satellite (GMS) Infrared (IR) data and ground-based observational data from X-band rain radar, equatorial atmosphere radar (EAR), L-band boundary layer radar (BLR), and upper-air sounding at Koto Tabang (KT: $100.32°$ E, $0.20°$ S, 865 m above mean sea level), West Sumatera.

In the analysis period, four super cloud clusters (SCCs; horizontal scale of 2,000-4,000 km), associated with an ISO, are seen to propagate eastward from the eastern Indian Ocean to Indonesian maritime continent. The SCCs are recognized as envelopes of convection, composed of meso-α-scale cloud clusters (MαCCs; horizontal scale of 500-1,000 km) propagating westward. When SCCs reach the Indonesian maritime continent, the envelopes disappear but MαCCs are clearly observed. Over Sumatera, the evolution and structure of a distinct MαCC are closely related to the organization of localized cloud systems with a diurnal cycle. The cloud systems are characterized by westward-propagating meso-β-scale cloud clusters (MβCCs; horizontal scale of ~100 km) developed in eastern Sumatera, and an orographic cloud system formed over a mountain range in western Sumatera.

Ground-based observation further revealed the internal structure of the orographic cloud system around KT. A meso-β-scale convective precipitation with eastward propagation (E-MβCP; horizontal scale of ~40 km) is found with the formation of the orographic cloud system. This is associated with a low-level wind change from easterly to westerly, considered to be local circulation over the

mountain range. The E-MβCP also indicates a multi-cell structure composed of several meso-γ-scale convective precipitations (MγCPs; horizontal scale of <10 km) with multiple evolution stages (formation, development and dissipation).

1. Introduction

Tropical cloud systems, associated with the intraseasonal oscillation (ISO), play an important role in driving the global atmospheric circulation through the release of latent heating. They are known as organized convective systems on a wide range of spatial and temporal scales, based on satellite observations (e.g., Nakazawa 1988; Lau et al. 1991; Sui and Lau 1992). Nakazawa (1988) showed the multi-scale structure of synoptic-scale convective systems in the convectively active phase of the ISO. Such synoptic-scale convective systems are termed super cloud clusters (SCCs). They are recognized as eastward-propagating envelopes of convection, composed of westward-propagating cloud clusters (CCs) in mesoscale.

Many authors pointed out that the evolution and movement of SCCs changed over large islands (Sumatera and Kalimantan) of the Indonesian maritime continent as they propagated from the eastern Indian Ocean to the western Pacific on the equator (e.g., Nitta et al. 1992; Seto et al. 2004; Welckmann and Khalsa 1990). Nitta et al. (1992) stated that an SCC decayed temporarily over the Indonesian maritime continent, because the associated westerly wind burst was blocked by the elevated topography of Sumatera, where is located at the western edge of the Indonesian maritime continent. Welckmann and Khalsa (1990) showed that a slowly-propagating SCC which resulted from quasi-stationary convection over the large islands.

In a recent paper, Seto et al. (2004) demonstrated westward-propagating CCs in an SCC that smoothly propagated over the Indonesian maritime continent. The propagation of CCs appears to be related to the diurnal oscillation of convection dominated in/around the large islands. In order to understand the evolution process of SCC and its interaction mechanism with the diurnal oscillation over the Indonesian maritime continent, we need to investigate further the internal structure of these convective systems using ground-based observations.

At Koto Tabang (hereafter KT: 100.32°E, 0.20°S, 865 m above mean sea level (MSL)), West Sumatera, an L-band boundary layer radar (BLR) has been operated since 1998, revealing a number of diurnal features of precipitation. Murata et al. (2002) reported that precipitation at KT tended to occur when the low-level wind was weak, while it did not appear when the low-level wind intensified. Renggono et al. (2001) investigated the diurnal variations of convective-type and stratiform-type precipitation classified by the vertical structure of the precipitation systems.

Recently, an X-band rain radar and a VHF-band wind profiler called the equatorial atmosphere radar (EAR) have been installed at KT, in addition to the BLR. These instruments enable us to study the structure and evolution of precipitation systems, and the vertical profile of wind field including vertical motion over the whole troposphere.

From 01 to 30 November 2002, the first combined observation using the X-band rain radar, EAR, BLR, and GPS radiosonde was performed at KT. During this period, Geostationary Meteorological Satellite (GMS) Infrared (IR) data showed the eastward propagation of four SCCs associated with an ISO over the eastern Indian Ocean and the Indonesian maritime continent. Convective

systems with various scales[1], shown in Table 1, are found within the SCCs in the satellite and ground-based observations. In this study, the temporal evolution and spatial change of convective systems at each scale are investigated in detail. The purpose of the present paper is to demonstrate the multi-scale aspects of convective systems over Sumatera in the convectively active phase of the ISO.

2. Observational data

2.1 Cloud system over the Indian Ocean and Indonesian maritime continent

This study uses hourly TBB (cloud top equivalent blackbody temperature) data from GMS-IR, recorded in longitude/latitude $0.05°$ grids. The TBB data in longitude/latitude 0.5 grids, averaged from the pixel data, are used to examine the characteristics of synoptic-scale and meso-α-scale cloud systems associated with the ISO from $70°$ E to $120°$ E. The fine (meso-β-scale) structure of meso-α-scale cloud systems is also studied using the pixel data.

2.2 Precipitation system around KT

Figure 1a presents the surface topography of the Indonesian maritime continent. A mountain range higher than 500 m is located along the western edge of Sumatera. The location of the EAR observatory at KT is shown by the plus mark (Fig. 1b). The height of the observatory is 865 m above MSL.

The X-band rain radar was used at the EAR observatory. The basic specification of the radar was described in Konishi et al. (1998). A volume scan data for reflectivity was acquired at 10-min intervals. Constant Altitude of Plan

---

[1] In this study, we refer the scale classification of convective systems to the scale definition of Orlanski (1975).

Position (CAPPI) data at an altitude of 3 km above MSL is used to examine the spatial structure of meso- β and - γ -scale precipitation systems. The observational range has a 32 km radius as shown by the circle in Fig. 1b, but the CAPPI data is mainly used in the rectangular area (60 km east-west and 30 km south-north) within the circle, because of the orographic shadows surrounding KT. At this site, surface rainfall was also measured by an optical rain-gauge at 1-min intervals.

2.3 Vertical profiles of wind, rain, temperature, and humidity at KT

At KT, two different types of wind profilers are operated with the X-band rain radar. One is a VHF-band wind profiler named EAR. This radar provides continuous vertical profiles of three components of the wind field with a fine resolution of ~90 sec in time and ~150 m in height over the whole troposphere (Fukao et al. 2003).

The other is an L-band wind profiler named BLR. This radar is located at a Global Atmosphere Watch (GAW) Station of the World Meteorological Organization (WMO), which is 200 m away from the EAR observatory. BLR obtains vertical profiles of horizontal wind, restricted in clear-air conditions to the boundary layer but increasing in rainy conditions to 6.4 km in height. Time and height resolutions are ~90 sec and ~100 m (Renggono et al. 2001). In this study, BLR data are used to examine the wind field below 1.5 km in height, which EAR cannot cover because of technical limitations. Reflectivity observed by BLR is also employed to investigate the vertical structure of precipitation systems.

During this study period, an upper sounding observation with GPS radiosonde

was also carried out at 3-hourly or 6-hourly intervals at the GAW station. To examine the atmospheric stratification, equivalent potential temperature (θ_e) is computed from pressure, temperature and humidity profile data. Vertical profiles of wind profiler and upper sounding data are shown, referenced to their altitude above MSL.

3. Overview of cloud systems associated with an intraseasonal oscillation

Figure 2 presents a longitude-time section of TBB averaged over $2°$S-$2°$N from 29 October to 23 November 2002. During this period, four SCCs with TBB of $-10°$C propagating eastward are observed over the eastern Indian Ocean, as shown by long arrows. Each SCC consists of individual meso-α-scale cloud clusters (MαCCs) with TBB of $-30°$C propagating westward. The horizontal scale of an SCC is 2,000-4,000 km, while that of an MαCC is 500-1,000 km. Successive SCCs are named SCC1, SCC2, SCC3, and SCC4.

The eastward propagation of SCCs becomes obscure as they reach Sumatera at ~$100°$E. It seems that the evolution of SCCs is influenced by the mountain range in western Sumatera, as pointed out by Nitta et al. (1992). However, westward-propagating MαCCs are clearly observed at 100-110$°$E. It is also noticeable that the diurnal variation of cloud activity is vigorous over Sumatera. The cloud activity indicates the occurrence and passage of westward-propagating MαCCs.

Figure 3a presents a time-altitude section of zonal wind observed by EAR at altitudes between 2.4 and 12.0 km at KT (shown by solid line in Fig. 2). Zonal wind of BLR data, averaged over altitudes of 1.4-2.4 km, and daily rainfall

amounts at KT are also shown in Figs. 3b and c, respectively. In our analysis, the local standard time (LST = UTC+7 hours) in Indonesia will be used from here on.

In Fig. 3a, an easterly wind is predominant until 19 November. During this period, the easterly wind in the lower troposphere weakens as SCCs arrive over KT. With the weakening of the easterly wind, a dominant westerly wind appears below an altitude of 2.4 km during the passage of SCC3 and SCC4 (Fig. 3b).

After 19 November, the low-level westerly wind significantly intensifies and ascends to an altitude of 5 km. The intense low-level wind in SCC4 is recognized as a westerly wind burst reported in previous study of developing SCC (e.g., Nitta et al. 1992).

In the present study, we focus on an MαCC on 10-11 November in association with SCC2, as a typical example of westward-propagating MαCCs over the Indonesian maritime continent. This MαCC is indicated by the rectangle in Fig. 2. The passage of the MαCC causes rainfall of 53 mm h^{-1} at KT on 10 November, and it is the maximum observed during the analysis period (Fig. 3c).

The temporal and spatial change of the MαCC over the Indonesian maritime continent is presented in Fig. 4. The propagation of the MαCC is indicated by the solid line. A meso-β-scale cloud system forms around the west coast of Kalimantan at 01 LST on 10 November, and it develops into an MαCC at 07 LST. The MαCC reaches eastern Sumatera at 13 LST, and it extends north-south over Sumatera and the Malay Peninsula by 19 LST. At 01 LST on 11 November, the MαCC separates into two cloud areas on the northern and southern sides of KT (shown by the plus mark). After that, these cloud areas disappear over the coastal region of western Sumatera (not shown here). It is evident that the

structure and propagation of this $M\alpha CC$ are related to the development of localized cloud systems with a diurnal cycle over the Indonesian maritime continent.

4 General features of $M\alpha CC$ over Sumatera

4.1 Meso-β-scale convective systems within an $M\alpha CC$

In this subsection, the fine structure of an $M\alpha CC$ over the equatorial region of Sumatera is described. Figure 5 presents 2-hourly maps of an $M\alpha CC$ from 11 to 23 LST on 10 November. The mountainous region higher than 500 m in western Sumatera is indicated by the shaded areas in the panel of 11 LST. Over Sumatera, the $M\alpha CC$ is regarded as a lump composed of meso-β-scale cloud clusters ($M\beta CCs$; horizontal scale of ~100 km) with TBB of -60~-50°C until 21 LST. $M\beta CCs$ develop successively in eastern Sumatera, and move west-southwestward. They are defined by βi, where i is the number of respective $M\beta CCs$. The movement and structure of $M\alpha CC$ are related to the evolution of $M\beta CCs$ as follows.

In the front part of the $M\alpha CC$, $\beta 1$ and $\beta 2$ occur over the east coast of Sumatera at 11 LST. At 13-15 LST, $\beta 1$ gradually weakens and $\beta 2$ develops while moving to western Sumatera. At 17 LST, when $\beta 1$ arrives the west coast of Sumatera, shallow clouds are distributed along the west foot of the mountain range. With the arrival of $\beta 2$ to the mountain range, the shallow clouds develop into an orographic cloud system at 19 LST.

In the central part of the $M\alpha CC$, $\beta 3$, $\beta 4$ and $\beta 5$ appear in/around the east coast of Sumatera at 15-17 LST. They sustain their activity while moving to

western Sumatera, and merge into the orographic cloud system over the mountain range at 19-21 LST. In the merging process, the MαCC alters into a wide-spreading orographic cloud system along the mountain range at 23 LST.

In the rear part of the MαCC, β6, β7, and β8 are located in eastern Sumatera at 17-19 LST. They move slower than the other MβCCs, and gradually decay over central Sumatera at 21-23 LST.

4.2 Meso-β-scale precipitation systems within the MαCC around KT

Figure 6a presents a time series of TBB from the pixel data at KT (100.3°E, 0.2°S) from 10 LST on 10 November to 04 LST on 11 November. At 16-18 LST on 10 November, the low TBB of below -30°C shows the appearance of shallow clouds. The lower TBB of ~ -50°C between 19-23 LST signifies the passage of MαCC. The internal structure of these cloud systems is investigated using the ground-based observational data.

Figure 6b presents the zonal movement of the maximum CAPPI echo over the region extending 15 km north and south of the radar site. The analysis area is shown in the rectangular box of Fig. 1b. At 12-14 LST, a group of intense precipitation echoes ($\geq$ 40 dBZ) appears around KT in a cloud with high TBB (0°C). Another group of intense precipitation echoes is seen 25-30 km west of the radar site, and shifts eastward with time, although each intense precipitation echo propagates westward. Its horizontal scale is ~40 km around KT. Thus, the group of intense precipitation echoes is defined as meso-β-scale convective precipitation (E-MβCP) with eastward propagation. Moderate precipitation echoes (30-39 dBZ) are also located to the rear of the E-MβCP. The E-MβCP

9

occurs with the formation of an orographic cloud system (see Fig. 5d).

After 19 LST, a meso-β-scale stratiform precipitation (<40 dBZ) with westward propagation (W-MβSP) appears at the passage of MαCC. The travel speed (~6 ms^{-1}) of W-MβSP is approximately twice as far as that of the E-MβCP moving in the opposite direction.

The movement of E-MβCP and W-MβSP is compared with the low-level zonal wind of BLR data averaged over altitudes of 1.4-2.4 km, where there is little influence from the environmental easterly wind (Fig. 6c). A low-level wind change from easterly to westerly occurs at 15 LST, when the front edge of the E-MβCP reaches the radar site. The low-level westerly wind is sustaining while the E-MβCP passes over the radar site. From this fact, it is inferred that the E-MβCP is accompanied by a low-level westerly wind from at least 30 km west of the radar site. The low-level westerly wind against the environmental easterly wind is considered to be local circulation over the mountain range. After that, the low-level wind changes to an easterly wind at the passage of W-MβSP.

4.3 Vertical structure of the E-MβCP and W-MβSP

Figure 7 presents time-altitude sections of (a) reflectivity obtained by BLR, (b) vertical velocity and (c) horizontal wind observed by EAR from 10 LST on 10 November to 04 LST on 11 November. In Fig. 7a, E-MβCP with a high reflectivity extending vertically is seen in the period of 15-19 LST on 10 November. It consists of two precipitation echoes separated by an echo-free region. The echo at 15 LST is the front edge of the E-MβCP, and it is associated with the change of the low-level wind from easterly to westerly (see Fig. 6c).

Another echo at 16-19 LST is the main part of the E-MβCP with the low-level westerly wind. It is accompanied by remarkable updrafts over a wide altitude range (Fig. 7b).

Between 20 LST on 10 November and 01 LST on 11 November, intermittent reflectively echoes with a melting layer at around an altitude of 4.5 km can be identified as W-MβSP. The height of the melting layer corresponds to the freezing level (~0°C) from the upper sounding data. In this period, weak updrafts and downdrafts are prominent above and below around altitude of 5 km, respectively. The vertical structures of the E-MβCP and W-MβSP mentioned above agree well with those of convective and stratiform portions, respectively, in the tropical squall line, as illustrated in Zipser (1977).

East-northeasterly and northeasterly winds are seen over altitude ranges of 4-10 km and below that, respectively, until 21 LST (Fig. 7c). The wind direction in the middle troposphere corresponds to the motion of MβCCs over Sumatera (see Fig. 5). In the E-MβCP, the environmental wind has almost uniform speed below an altitude of 8 km. Meanwhile, in the W-MβSP, it prevails above an altitude of 6 km and weakens below that in association with the passage of an MαCC.

Figure 8 presents a time-altitude section of equivalent potential temperature (θ_e) derived from the upper-air sounding data at KT. Below an altitude of 4 km, atmospheric stratifications in the E-MβCP and W-MβSP are nearly neutral with high θ_e (> 342 K) and weak convective instability, respectively. At altitudes of 4-7 km, θ_e increases at the passage of the MαCC after 19 LST on November.

A high θ_e region around the surface is also seen at 10 and 13 LST, before the

appearance of the E-MβCP. It is expected that the high θ_e cause a low-level westerly wind in association with the E-MβCP, through a thermal contrast between the mountain area and its surrounding area.

5. Meso-γ-scale convective precipitation systems within the E-MβCP

Figure 9 presents temporal and spatial changes of E-MβCP at 10-min intervals from 1600 to 1920 LST on 10 November. This figure indicates that the E-MβCP consists of several meso-γ-scale convective precipitations (MγCPs; horizontal scale of <10 km), which align approximately east-west. They are named γi, where i is the number of the respective MγCPs. The E-MβCP shifts gradually southward in association with the southwestward propagation of each MγCP as shown by solid lines. The propagation of MγCP is associated with the environmental wind in the lower troposphere (see Fig. 7c). The horizontal wind averaged over altitudes of 1.4-2.4 km is frequently southwesterly wind as shown by the arrow at the radar site (the plus mark), and the MγCPs have a southwest-northeast oriented structure in the low-level wind.

It is interesting that new MγCPs form successively to the east of the E-MβCP. While an MγCP propagates westward, it develops in the central portion of the E-MβCP and decays on the western edge. The lifetime of MγCPs is quite short (< 1 hour). As a result, a regular replacement of MγCPs occurs in the E-MβCP. After 1910 LST, it seems that the E-MβCP disappears with the approach of W-MβSP from the east.

During the passage of E-MβCP over KT, the vertical structure of MγCPs (γ2-6 and γ8) was observed by EAR and BLR. Figures 10a and b present

time-altitude sections of reflectivity and zonal-vertical wind. Time series of the low-level zonal wind and surface rainfall are also shown in Figs. 10c and d, respectively. In order to examine the kinematic structure of the E-MβCP relative to the environmental wind and local circulation, the zonal wind in Figs. 10b and c is subtracted from the mean wind at each altitude in this period. Considering the time series from right to left, the figures are regarded as the zonal structure of E-MβCP.

The vertical structure of reflectivity and vertical motions in the E-MβCP indicates a multi-cell structure composed of MγCPs with multiple evolution processes. The evolution of MγCPs is divided into formation, development, and dissipation stages in the life cycle of a single cell, as illustrated in Burgess and Lemon (1990). The features of MγCP at each evolution stage are described below.

Formation stage (from 1610 to 1655 LST): Two shallow precipitation echoes (γ2 and γ3) below altitudes of 4-5 km are seen at 1615 and 1650 LST, which are accompanied by updrafts at an altitude of around 2.5 km. The updrafts result in a convergent flow between easterly and westerly wind components at low levels.

Development stage (from 1655 to 1805 LST): A moderate precipitation echo more than 30 dBZ appears up to an altitude of 5.5 km. Intense precipitation echoes more than 40 dBZ (γ4 and γ5) are embedded within the precipitation echo. A light precipitation echo more than 20 dBZ (γ6) extends up to altitudes higher than 7 km. In γ4 and γ5, intense precipitation of 40-70 mm h^{-1} occurs at the surface. A strong updraft coexists with the convergent flow of the zonal wind component, and its region ascends with time. In γ6, updrafts are located over

altitudes between 6 and 8 km. At low levels, a gusty flow of the prevailing westerly wind component blows toward the front edge of the precipitation region, acting as a trigger to generate the low-level updraft within $\gamma 3$.

Dissipation stage (from 1805 to 1900 LST): In this stage, the top level of a light precipitation echo ($\gamma 8$) is seen at around an altitude of 5 km. Updraft regions are seen just above the echo top. A moderate precipitation echo coexists with downdrafts in $\gamma 8$. The low-level wind indicates a divergent flow that changed from a westerly to an easterly wind component in relation to the downdraft in the lower troposphere.

6. Characteristics of convective precipitations over the mountain range in western Sumatera

In this section, we describe the diurnal variation of convective precipitations around KT and its relation to SCC and MαCC. Figure 11a presents a local time-day section of echo areas of intense precipitation (≥ 40 dBZ), averaged at 1-hour intervals from 05 to 21 November. The echo area is calculated over the whole observational area shown by the circle in Fig. 1b. The diurnal variation of echo area summing up the 1-hour interval data for this period is also shown in Fig. 11b.

In Fig. 11a, large echo areas of intense precipitation lasting for 3-6 hours are seen on 06-07, 09-11, 13, and 17-18 November. The peak time of the total echo area in Fig. 11b is at 16 LST. The intense precipitation echoes occur as an environmental easterly wind weakens in the lower troposphere at the passage of SCCs (see Fig. 3b).

Next the low-level wind behaviors in relation to convective precipitations are

14

investigated. Low-level zonal winds averaged at altitudes of 1.4-2.4 km at 6-hourly intervals during the analysis period are listed in Table 2. The periods of dominant easterly and westerly winds at low levels, shown in Fig. 3b, are defined as easterly and westerly wind phases, respectively.

In the easterly wind phase, the decrease of a low-level easterly wind and the change of that to westerly wind are seen between 10 and 16 LST. The diurnal changes of low-level zonal wind, considered to be local circulation, are associated with the occurrence of the large echo area of intense precipitation. When intense precipitation echoes are accompanied by the low-level westerly wind (10 and 17 November), they are identified as an E-MβCP. Meanwhile, intense precipitation echoes are not observed in the westerly wind phase, except on 18 November.

Westward-propagating MαCCs are also observed over Sumatera in almost convective precipitation events, as schematically illustrated in Fig. 12. While an MαCC develops over central and eastern Sumatera, convective precipitations appear with the formation of an orographic cloud system over the mountain range. When the MαCC reaches the mountain range, precipitation features around KT changes from convective to stratiform type due to the change of an environmental wind (see Figs. 6c and 7c).

The diurnal variation of convective precipitations in relation to the formation of the orographic cloud system around KT is consistent with the one of intense rainfall area dominated along the mountain range shown by Mori et al. (2004), from TRMM (Tropical Rainfall Measuring Mission) precipitation radar data.

Murata et al. (2002) pointed out that the evolution of localized cloud systems in relation to local circulation over Sumatera was controlled by the strength of

environmental wind at altitudes of 1-2 km, from the comparison of cloud map and BLR data at KT. In our study, it is inferred that the weakening of lower-tropospheric environmental wind associated with SCCs provides a favorable condition for the formation and development of the orographic cloud system due to distinct local circulation over the mountain range.

7. Concluding remarks

  In the present study, we investigated the behavior and evolution of convective systems with various scales (synoptic-scale and meso-α, β, γ-scale) over the Indonesian maritime continent in the convectively active phase of an intraseasonal oscillation (ISO) during November 2002, using Geostationary Meteorological Satellite (GMS) Infrared (IR) data and ground-based observational data from X-band rain radar, equatorial atmosphere radar (EAR), boundary layer radar (BLR), and upper-air sounding at Koto Tabang (KT), West Sumatera. The multi-scale aspects of convective systems associated with the ISO are summarized as follows.

(1) In the analysis period, four super cloud clusters (SCCs) propagating eastward are observed over the eastern Indian Ocean and the Indonesian maritime continent. They are recognized as envelopes of convection, composed of meso-α-scale cloud clusters (MαCCs) propagating westward. When SCCs reach Sumatera, the envelopes disappear, but the MαCCs are evident over the region from Sumatera to Kalimantan.

(2) Over Sumatera, the evolution and structure of a distinct MαCC are related to the organization of localized cloud systems with a diurnal cycle. The cloud systems are characterized by westward-propagating meso-β-scale cloud clusters

(MβCCs) developed over eastern Sumatera, and an orographic cloud system formed over the mountain range in western Sumatera. While the MαCC crosses over Sumatera, its structure changes from an organized cloud system consisting of MβCCs into a developing orographic cloud system over the mountain range.

(3) Ground-based observations revealed the internal structure of the orographic cloud system around KT. A meso-β-scale convective precipitation with eastward propagation (E-MβCP) is observed with the formation of the orographic cloud system. It is accompanied by a low-level westerly wind against an environmental easterly wind, considered to be local circulation over the mountain range. A meso-β-scale stratiform precipitation with westward propagation (W-MβSP) is also observed in the development of the orographic cloud system into the MαCC.

(4) The E-MβCP indicates a multi-cell structure composed of several meso-γ-scale convective precipitations (MγCPs), which align approximately east-west. Successive formation of MγCPs occurs to the east of the E-MβCP by a low-level convergent flow. Each MγCP propagates westward, progressing through multiple stages (formation, development, and dissipation). The regular replacement of MγCPs plays a principal role in the movement and maintenance of the E-MβCP.

Through the analysis period, convective precipitations occur around KT as a lower-tropospheric easterly wind weakens at the passage of SCCs. They are also associated with a diurnal variation of low-level zonal wind. From these results, it is inferred that the environmental wind associated with SCCs provides a favorable condition for the development of localized convective systems, which leads to the formation of MαCCs, due to local circulations (i.e., valley-mountain

and sea-land breezes) over the Indonesian maritime continent.

In this study, we demonstrated the complicated evolution of precipitation systems and the associated wind behavior at the passage of SCCs, but the analysis area of precipitation and wind is limited in/around KT. In the future work, we will further study the influence of Sumatera's topography on the environmental wind associated with SCCs, and the interaction process of SCCs with localized convective systems over the whole region of Sumatera, with both of observation and numerical model studies.

References

Burgess, D. W., and L. R. Lemon, 1990: Severe thunderstorm detection by radar, in *Radar in Meteorology: Battan Memorial and 40th Anniversary Radar*

Meteorology Conference, edited by D. Atlas, American Meteorology Society, 619-647.

Fukao, S., H. Hashiguchi, M. Yamamoto, T. Tsuda, T. Nakamura, M. K. Yamamoto, T. Sato, M. Hagio, and Y. Yabugaki, 2003: Equatorial atmosphere radar (EAR): System description and first results. *Radio Sci.*, *38(3)*, **1053**, doi:10.1029/2002RS002767.

Konishi, H., M. Wada, and T. Endoh, 1998: Seasonal variations of cloud and precipitation at Syowa station, Antarctica. *Ann. Glaciol.*, **27**, 597-602.

Lau, K., Nakazawa T., and Sui C. H., 1991: Observations of cloud cluster hierarchies over the tropical western Pacific, *J. Geophys. Res.*, **96**, 3197-3208.

Mori, S., J. Hamada, Yudi I. T., M. D. Yamanaka, N. Okamoto, F. Murata, N. Sakurai, H. Hashiguchi, and T. Sribimawati, 2004: Diurnal land-sea rainfall peak migration over Sumatera Island, Indonesian maritime continent observed by TRMM satellite and intensive rawinsonde soundings, *Mon. Wea. Rev.*, **132**, 2021-2039.

Murata, F., M. D. Yamanaka, M. Fujiwara, S.-Y. Ogino, H. Hashiguchi, S. Fukao, M. Kudsy, T. Sribimawati, S. W. B. Harijiono, and E. Kelana, 2002: Relationship between wind and precipitation observed with a UHF radar, GPS rawinsondes and surface meteorological instruments at Kototabang, west Sumatera during September-October., *J. Meteor. Soc. Japan*, **80**, 347-360.

Nakazawa, T., 1988: Tropical super cloud clusters within intraseasonal variations over the western Pacific. *J. Meteor. Soc. Japan*, **66**, 823-839.

Nitta, Ts., T. Mizuno and K. Takahashi, 1992: Multi-scale convective systems during the initial phase of the 1986/87 EI Nino. *J. Meteor. Soc. Japan*, **70**, 447-466.

Orlanski, J., 1975: A rational subdivision of scales for atmospheric process. *Bull Amer. Met. Soc.*, **56**, 527-530.

Renggono, F., H. Hashiguchi, S. Fukao, M. D. Yamanaka, S.-Y. Ogino, N. Okamoto, F. Murata, B. P. Sitorus, M. Kudy, M. Kartasasmita, and G. Ibrahim, 2001: Precipitating clouds observed by 1.3-GHz boundary layer radars in equatorial Indonesia, *Ann. Geophys.*, **19**, 889-897.

Seto, T. H., M. K. Yamamoto, H. Hashiguchi, and S. Fukao, 2004: Convective activities associated with intraseasonal variation over Sumatera, Indonesia observed with the equatorial atmosphere radar, *Ann. Geophys.*, **22**, 3899-3916.

Sui, C.-H, and K.-M. Lau, 1992; Multiscale phenomena in the tropical atmosphere over the Western Pacific, *Mon. Wea. Rev.*, **120**, 407-430.

Welckmann, K. M. and S. J. S. Khalsa, 1990: The shift of convection from the Indian Ocean to the Western Pacific Ocean during a 30-60 day oscillation, *Mon. Wea. Rev.*, **118**, 964-976.

Zipser, E. J., 1977: Mesoscale and convective-scale downdrafts as distinct components of squall-line circulation, *Mon., Wea. Rea.*, **108**, 1568-1589.

Figure Captions

Fig. 1: (a) Surface topography of the Indonesian maritime continent. The map in panel b is magnified from the square area in panel a. A plus mark is the location of the EAR observatory. The circle marks the observational area of the X-band rain radar. The X-band radar data is mainly used in the rectangular area within the circle, because of the orographic shadows surrounding KT.

Fig. 2: Longitude-time section of 6-hourly TBB averaged over 2°S-2°N from 29

October to 23 November 2002. The propagation of SCCs is indicated by long arrows. The solid line is the longitude of KT. The cloud system in the rectangle is a westward-propagating MαCC on 10-11 November.

Fig. 3: (a) Time-altitude section of zonal wind observed by EAR, and time series of (b) low-level zonal wind from BLR data averaged at altitudes between 1.4 and 2.4 km, and (c) daily rainfall amount at KT during 01-23 November 2002. The time average of zonal wind data obtained from EAR and BLR is 3 hours.

Fig. 4: 6-hourly maps of TBB averaged over longitude/latitude 0.5° grids over the maritime continent from 01 LST on 10 November to 01 LST on 11 November. The propagation of an MαCC is indicated by a solid line. The location of the radar site is shown by the plus mark.

Fig. 5: 2-hourly maps of pixel TBB data in/around Sumatera from 11 LST to 23 LST on 10 November. The mountainous region higher than 500 m is indicated by the shaded area in the top figure of 11 LST. The plus mark is the location of the radar site. The propagation of MβCCs is indicated by solid lines.

Fig. 6: Time series of (a) 1-hourly pixel TBB data at KT, (b) east-westward maximum CAPPI data over the region extending 15 km north and south of the radar site, and (c) the low-level zonal wind of the BLR data averaged over altitudes of 1.4-2.4 km from 10 LST on 10 November to 04 LST on 11 November. The time average of zonal wind data is 30 min. The propagation of both E-MβCP and W-MβSP is indicated by the wide arrow.

Fig. 7: Time-altitude sections of (a) reflectivity observed by BLR, and (b)

vertical velocity and (c) horizontal wind obtained by EAR from 10 LST on 10 November to 04 LST on 11 November. The time average of reflectivity and vertical velocity data is 10 min, while that of horizontal wind data is 1 hour.

Fig. 8: Time-altitude section of equivalent potential temperature (θ_e) observed by the upper-air sounding at intervals of 3 hours from 10 LST on 10 November to 04 LST on 11 November. In the bottom of the panel, the observational time of upper sounding is shown by arrows.

Fig. 9: Horizontal distribution of E-MβCP at 10-min intervals from 1600 to 1920 LST on 10 November. The propagation of MγCPs is indicated by solid lines. The plus mark is the radar site. Arrows shown at the radar site are the low-level wind averaged over altitudes of 1.4-2.4 km from BLR data.

Fig. 10: Time-altitude sections of (a) reflectivity from BLR data and (b) zonal-vertical wind from EAR data between 1600 and 1900 LST 10 November. Time variations of (c) the low-level zonal wind of BLR data and (d) surface rainfall in the same period. Zonal wind in panels b and c is subtracted from the mean wind at each altitude during this period to investigate the kinematic structure of the E-MβCP. The time series in these figures is from right to left in order to consider the east-westward structure of the E-MβCP. In panel c, arrows show the low-level convergent and divergent flows. The time averages of reflectivity, zonal-vertical wind, and the low-level zonal wind data are 2, 10, and 5 min, respectively.

Fig. 11: (a) Local time-day section of intense precipitation echoes (≥ 40 dBZ) averaged at 1-hour intervals from 05 to 21 November. (b) Diurnal variation of echo area summing up the 1-hour interval data during this analysis period. The echo area is calculated over the whole observational area shown by the circle in Fig. 1b.

Fig. 12: Schematic illustration of a westward-propagating MαCC over Sumatera and precipitation systems within an orographic cloud system over the mountain range in western Sumatera.

Table 1: Synoptic- and meso-scale convective systems associated with the ISO.

Convective systems	Horizontal scale
Super cloud cluster	2,000-4,000 km
Meso-α-scale cloud cluster	500-1,000 km
Meso-β-scale cloud cluster	~100 km
Meso-β-scale convective precipitation	~40 km
Meso-γ-scale convective precipitation	<10 km

Table 2: Low-level zonal wind averaged over altitudes of 1.4-2.4 km at 6-hourly intervals, and the low-level zonal wind phase from 05 to 21 November. Date and wind speed in convective precipitation events are indicated by the bold font.

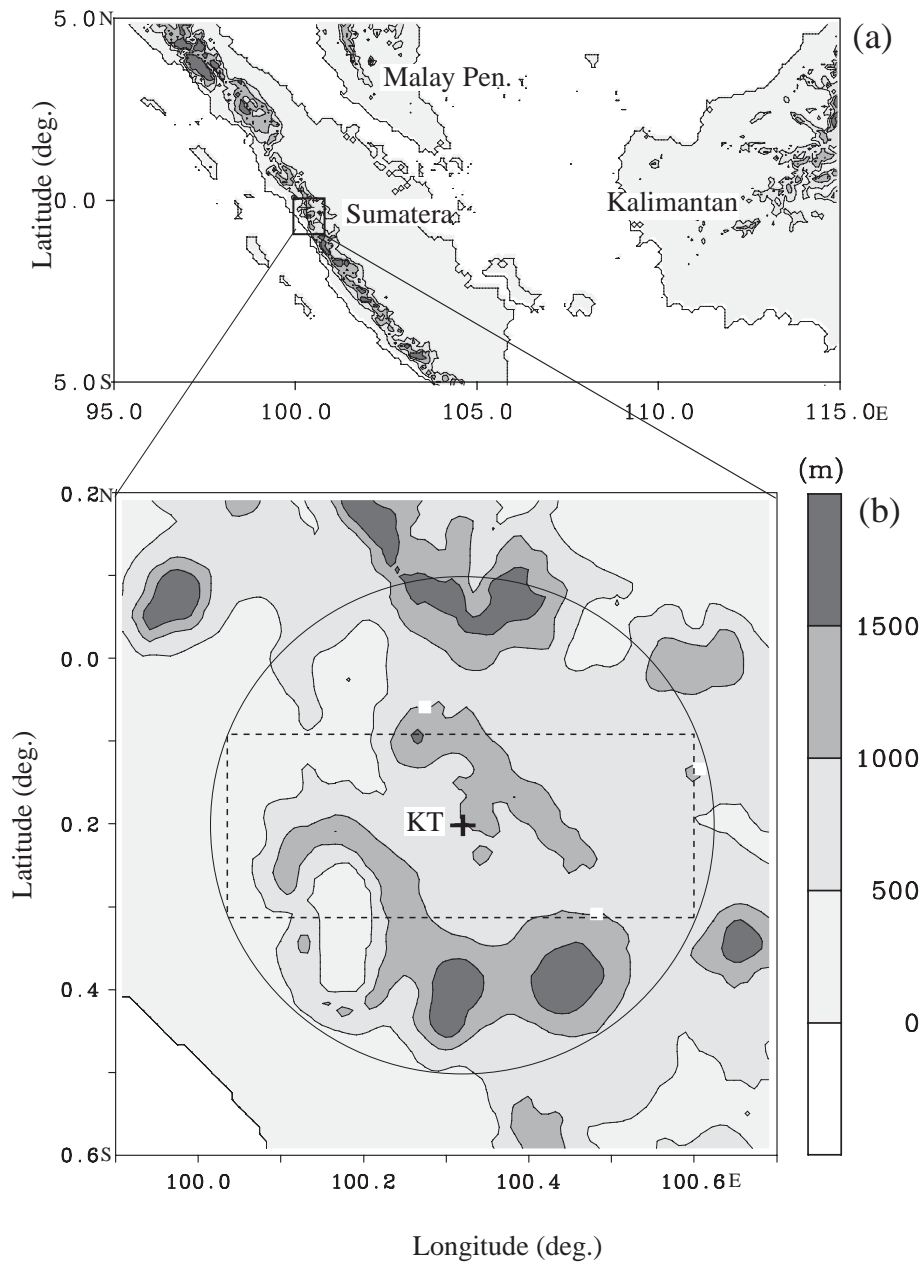| Date	Low-level zonal wind (m/s)				Low-level zonal wind phase
	04 LST	10 LST	16 LST	22 LST	
05 Nov	-1.4	-4.2	-1.7	-1.7	Easterly wind phase
06 Nov	**-0.7**	**-1.8**	**-1.3**	**-0.1**	
07 Nov	**-1.2**	**-3.2**	**-3.1**	**0.0**	
08 Nov	-2.2	-2.0	-3.8	-4.4	
09 Nov	**-6.2**	**-3.3**	**-1.5**	**-0.3**	
10 Nov	**-0.7**	**-2.0**	**2.7**	**-3.4**	
11 Nov	**-1.4**	**-6.0**	**-1.6**	**-1.5**	
12 Nov	-2.3	-5.9	-3.1	0.1	
13 Nov	**-0.4**	**-2.7**	**-1.1**	**0.0**	
14 Nov	3.7	3.1	0.7	-0.7	Westerly wind phase
15 Nov	0.8	0.0	3.0	-0.8	
16 Nov	**-1.5**	**-2.3**	**-1.6**	**-3.8**	Easterly wind phase
17 Nov	**-0.1**	**-1.0**	**2.6**	**-0.2**	
18 Nov	**-0.1**	**0.4**	**4.4**	**1.3**	Westerly wind phase
19 Nov	-0.5	2.4	1.9	0.1	
20 Nov	-0.3	1.1	7.9	11.5	
21 Nov	3.3	9.2	8.6	9.4	

Fig. 1: (a) Surface topography of the Indonesian maritime continent. The map in panel b is magnified from the square area in panel a. A plus mark is the location of the EAR observatory. The circle marks the observational area of the X-band rain radar. The X-band radar data is mainly used in the rectangular area within the circle, because of the orographic shadows surrounding KT.
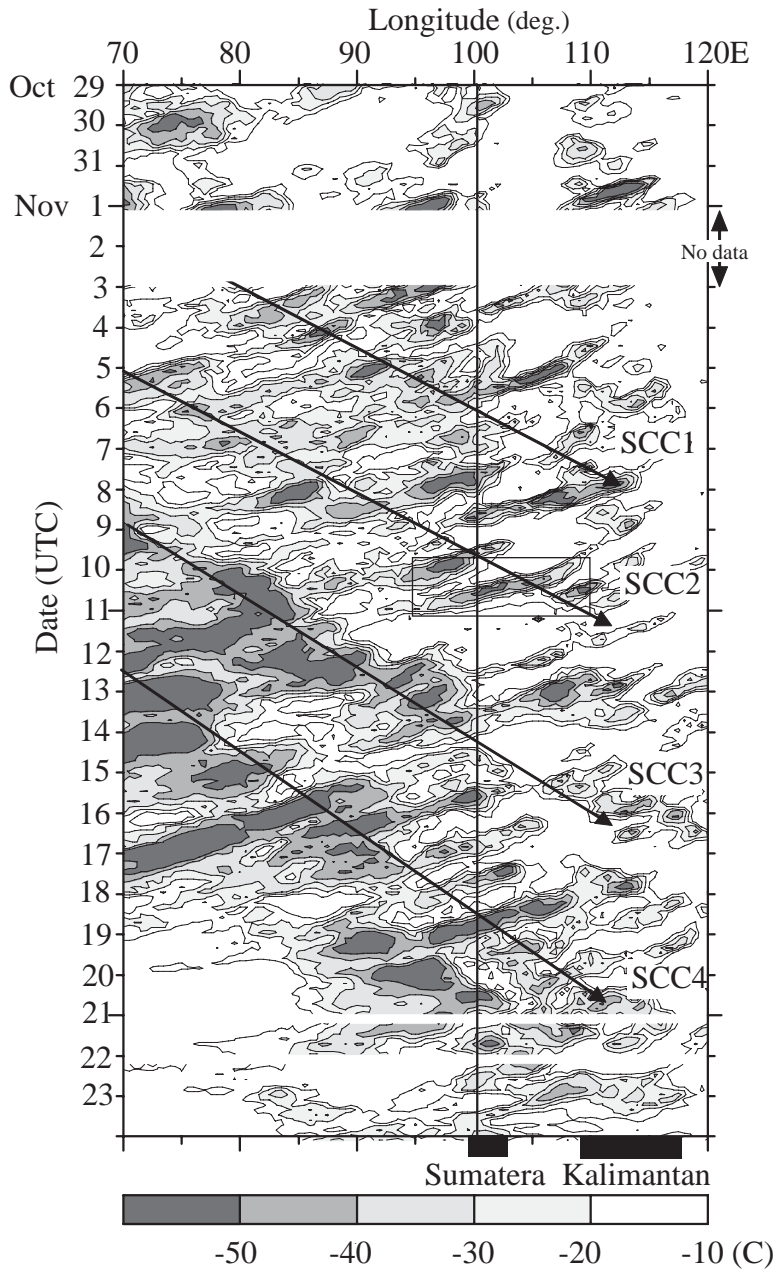
Fig. 2: Longitude-time section of 6-hourly TBB averaged over 2°S-2°N from 29 October to 23 November 2002. The propagation of SCCs is indicated by long arrows. The solid line is the longitude of KT. The cloud system in the rectangle is a westward-propagating MαCC on 10-11 November.

Fig. 3: (a) Time-altitude section of zonal wind observed by EAR, and time series of (b) low-level zonal wind of BLR data averaged at altitudes between 1.4 and 2.4 km, and (c) daily rainfall amount at KT during 01-23 on November 2002. The averaged time of zonal wind data obtained from EAR and BLR is 3 hours.
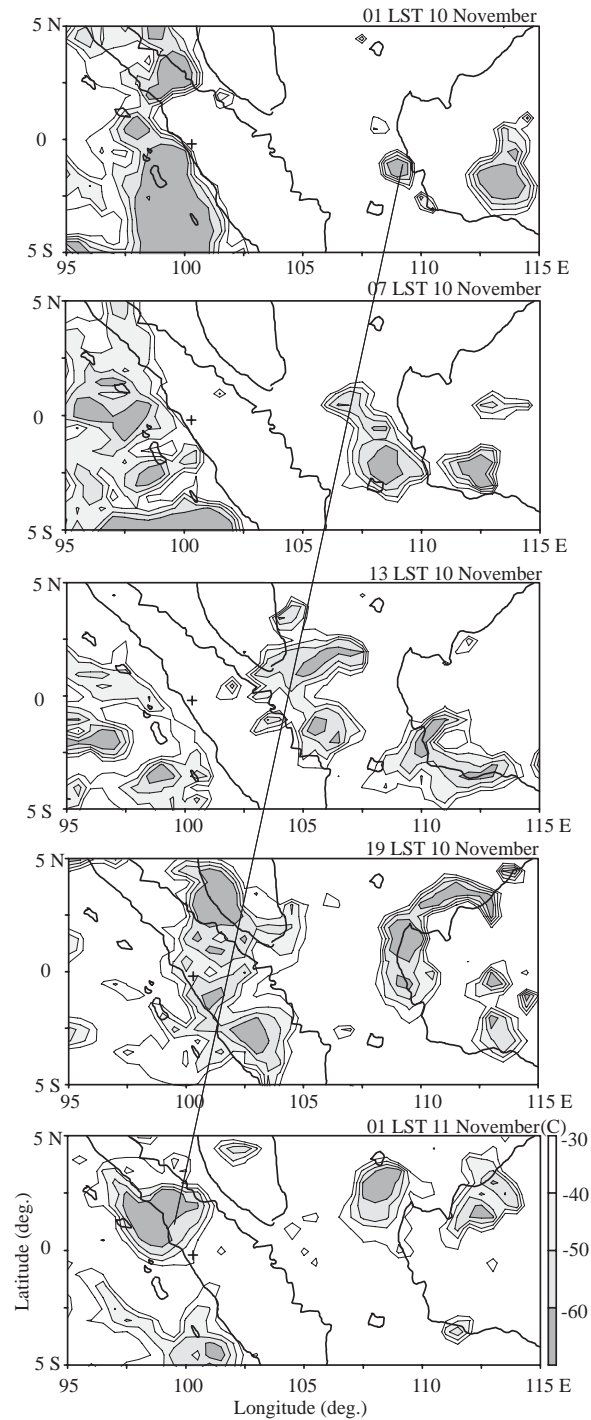
Fig. 4: 6-hourly maps of TBB averaged over longitude/latitude 0.5 ° grids over the maritime continent from 01 LST 10 to 01 LST 11 on November. The propagation of MαCC is indicated by the long arrow. The location of the radar site is shown by the plus mark.
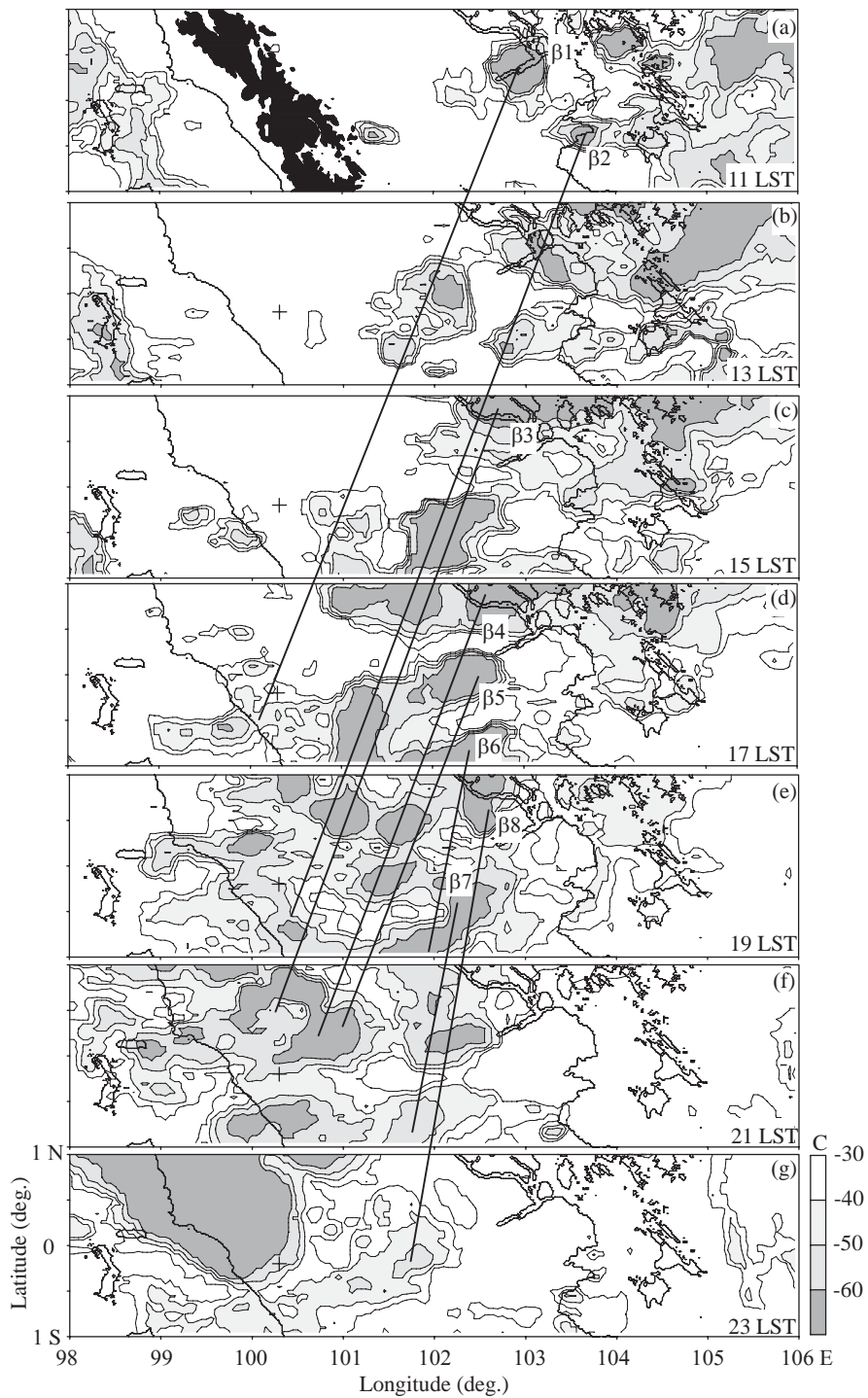
Fig. 5: 2-hourly maps of pixel TBB data in/around Sumatera from 11 LST to 23 LST on 10 November. The mountain range higher than 500 m is indicated by the shaded area in the top figure of 11 LST. The plus mark is the location of the radar site. The propagation of MβCCs is indicated by solid lines.
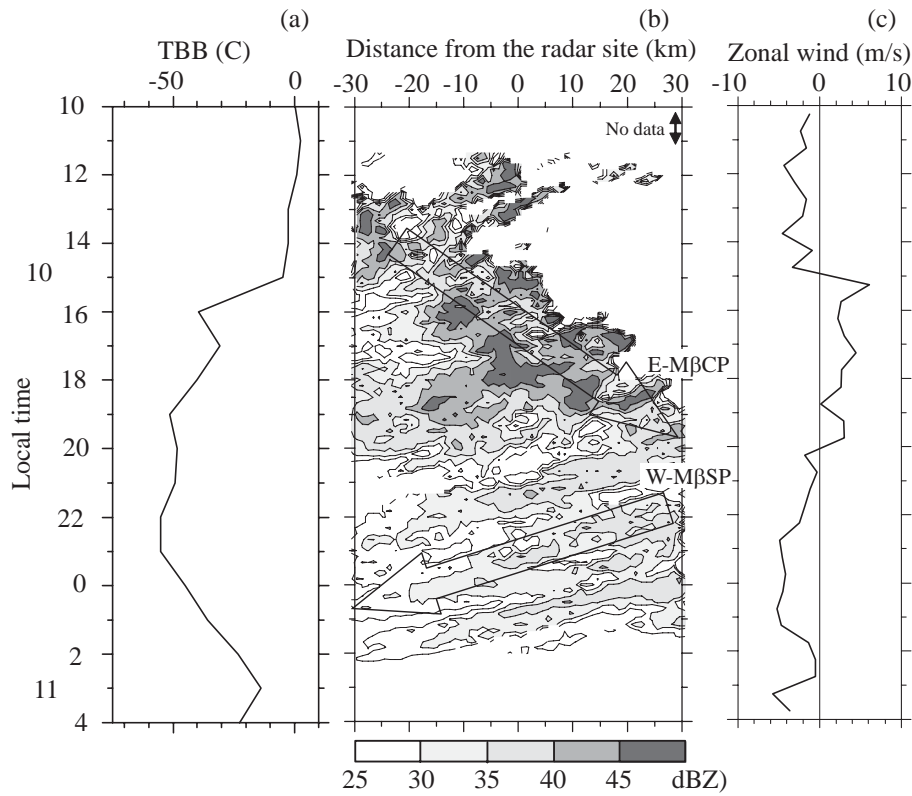
Fig. 6: Time series of (a) 1-hourly pixel TBB data at KT, (b) east-westward maximum CAPPI data over the region extending 15 km north and south of the radar site, and (c) the low-level zonal wind of BLR data averaged over altitudes of 1.4-2.4 km from 10 LST on 10 November to 04 LST on 11 November. The averaged time of zonal wind data is 30 min. The propagations of the E-MβCP and W-MβSP are indicated by the wide arrow.
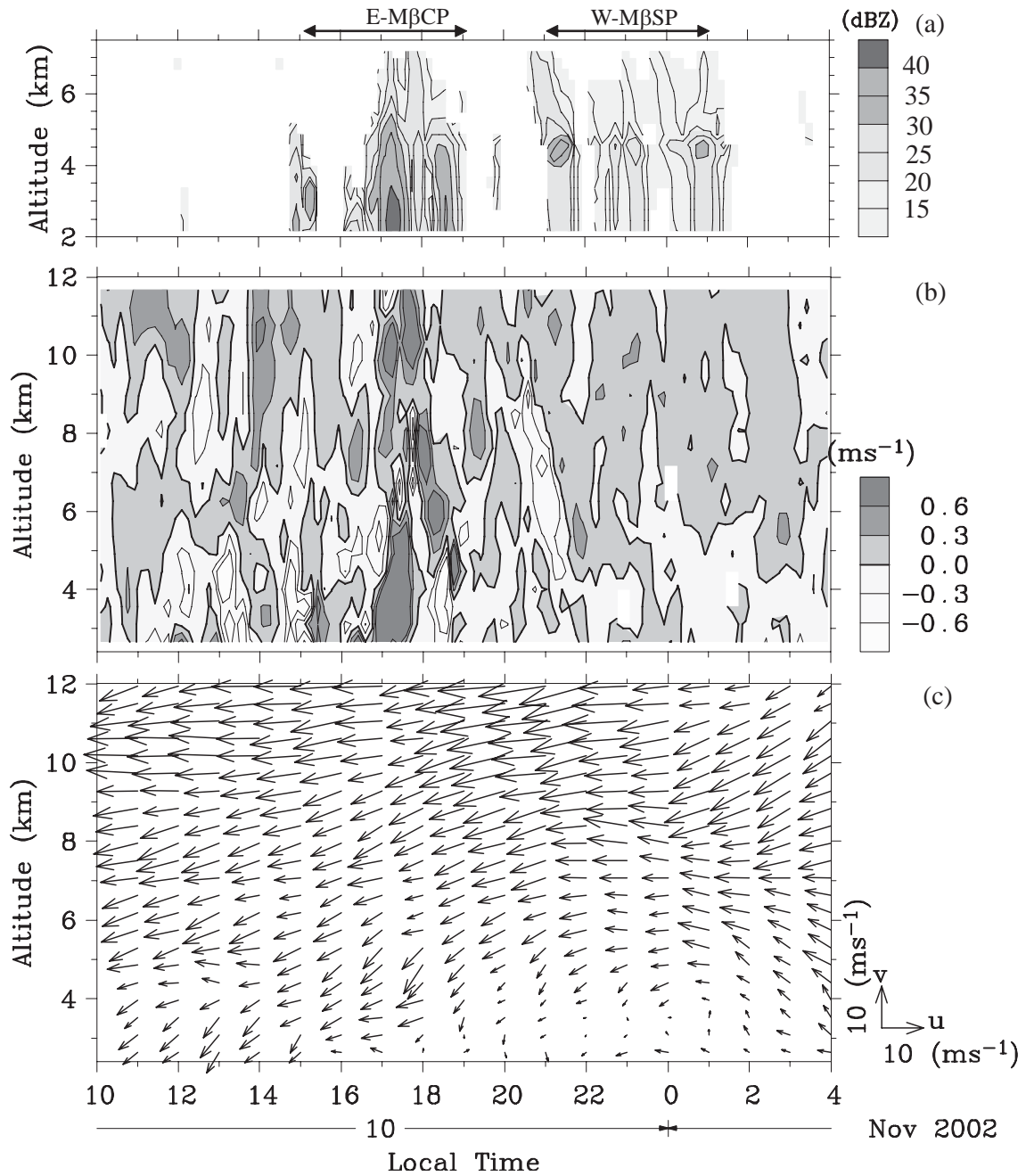
Fig. 7: Time-altitude sections of (a) reflectivity observed by BLR, and (b) vertical velocity and (c) horizontal wind obtained by EAR from 10 LST 10 to 04 LST 11 November. The averaged time of reflectivity and vertical velocity data is 10 min, while that of horizontal wind data is 1 hour.
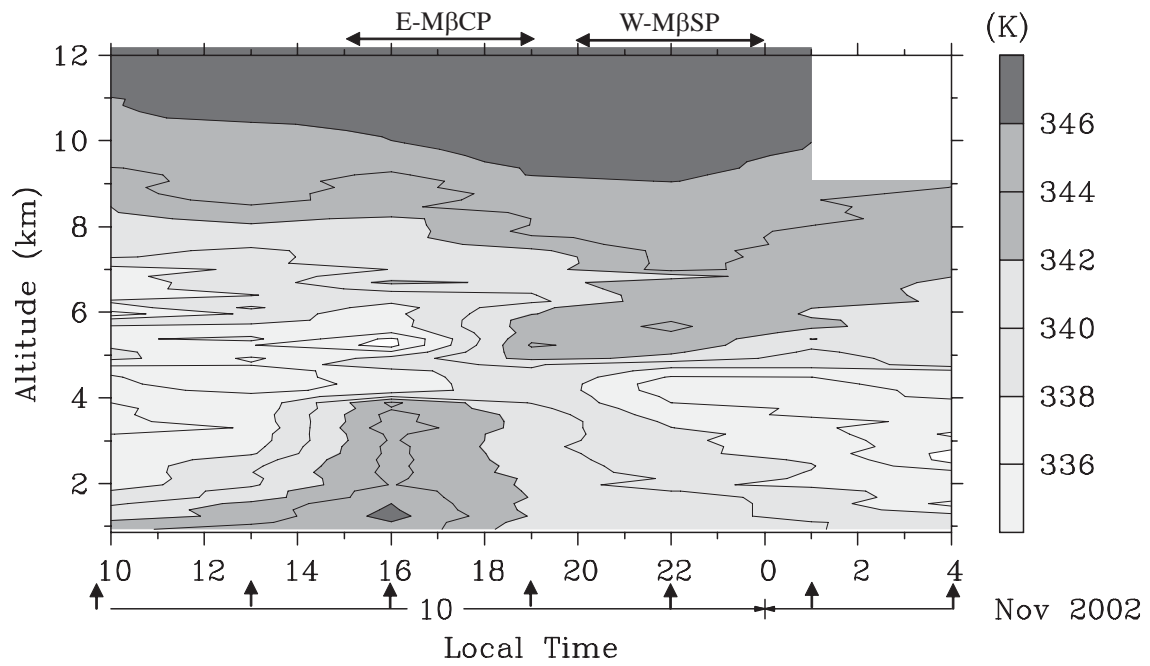
Fig. 8: Time-altitude section of equivalent potential temperature (θ_e) observed by the upper sounding at intervals of 3 hours from 10 LST 10 on November to 04 LST 11 on November. In the bottom of the panel, the observational time of upper sounding is shown by arrows.
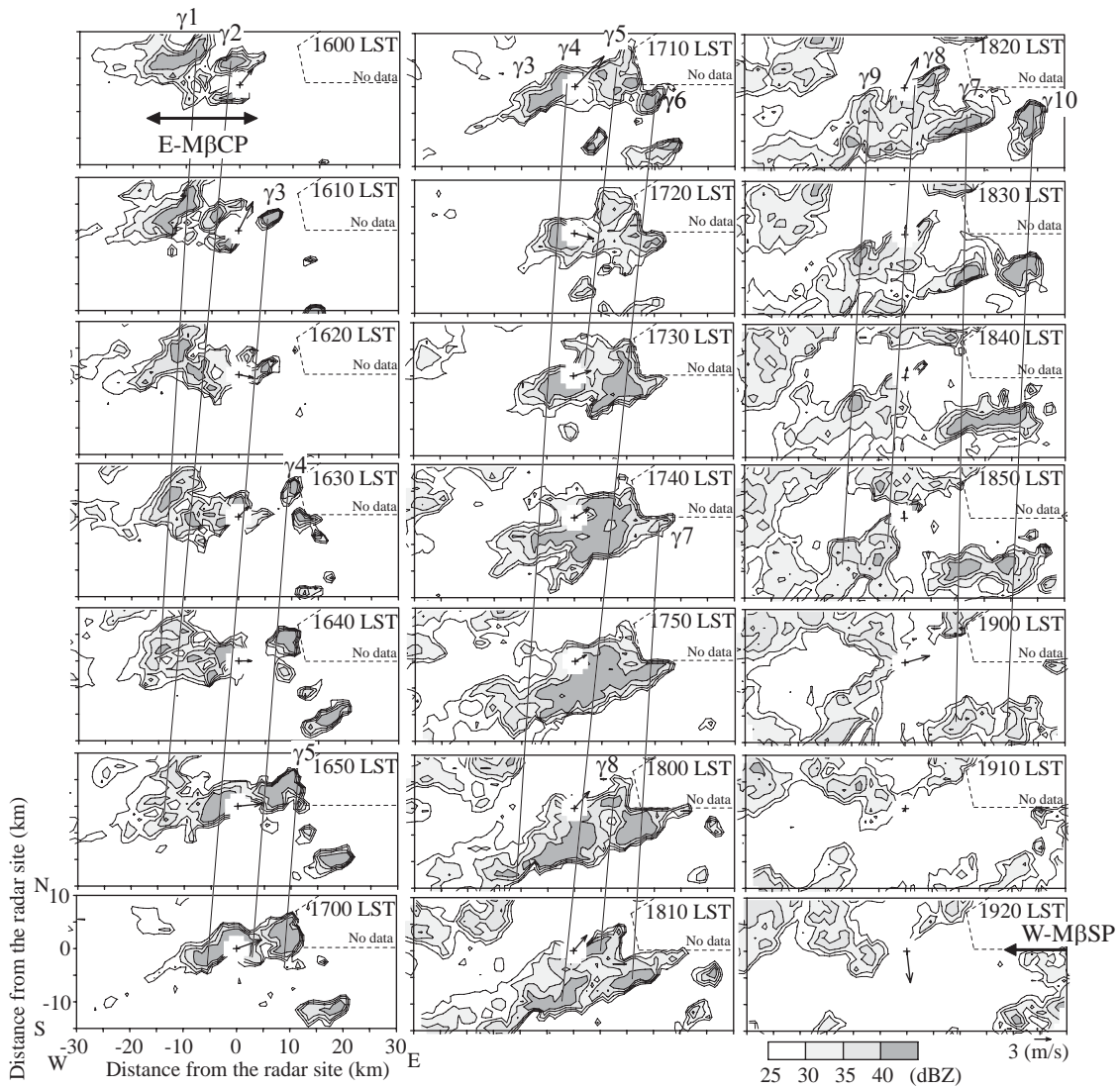
Fig. 9: Horizontal distribution of E-MβCP at intervals of 10 min from 1600 to 1920 LST on 10 November. The propagation of MγCPs is indicated by solid lines. The plus mark is the radar site. Arrows shown at the radar site are the low-level wind averaged over altitudes of 1.4-2.4 km from BLR data.

Dissipation stage   Development stage   Formation stage

(a) (dBZ)

40
35
30
25
20
15

γ8   γ6   γ5   γ4   γ3   γ2

19   18   17   16

10

(b)

2 (ms⁻¹)

w
u
10 (ms⁻¹)

19   18   17   16
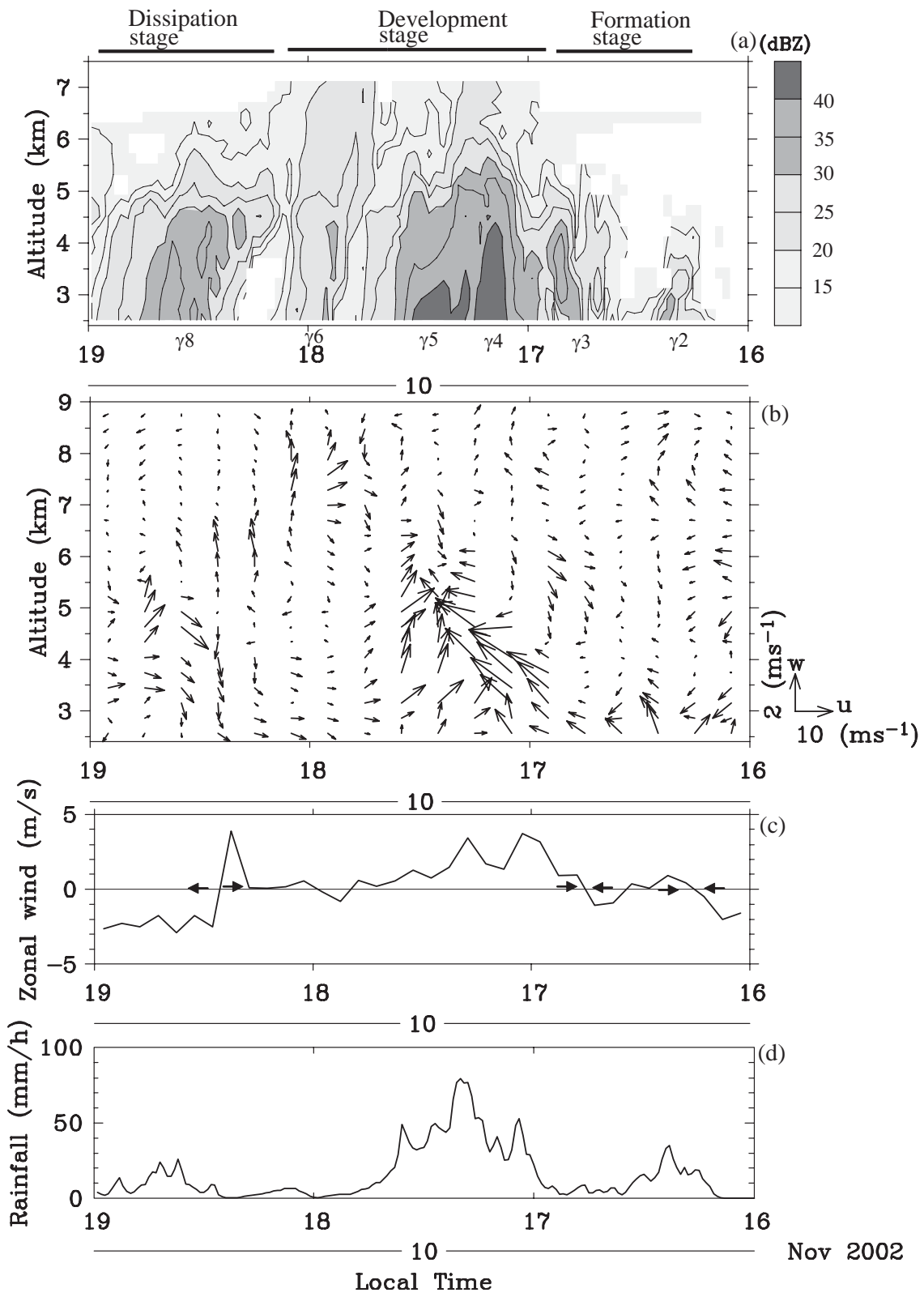
10

(c)

10

(d)

Nov 2002

Local Time

Fig. 10: Time-altitude sections of (a) reflectivity of BLR data and (b) zonal-vertical wind of EAR data from 1600 to 1900 LST on 10 November. Time variations of (c) the low-level zonal wind of BLR data and (d) surface rainfall in the same period. Zonal wind in panels b and c are subtracted from the mean wind at each altitude during this period to investigate the kinematic structure of the E-MβCP. The time series in these figures is indicated in the direction from right to left in order to consider the east-westward structure of the E-MβCP. In panel c, arrows show the low-level convergent and divergent flows. The averaged times of reflectivity, zonal-vertical wind, and the low-level zonal wind data are 2, 10, and 5 min, respectively.
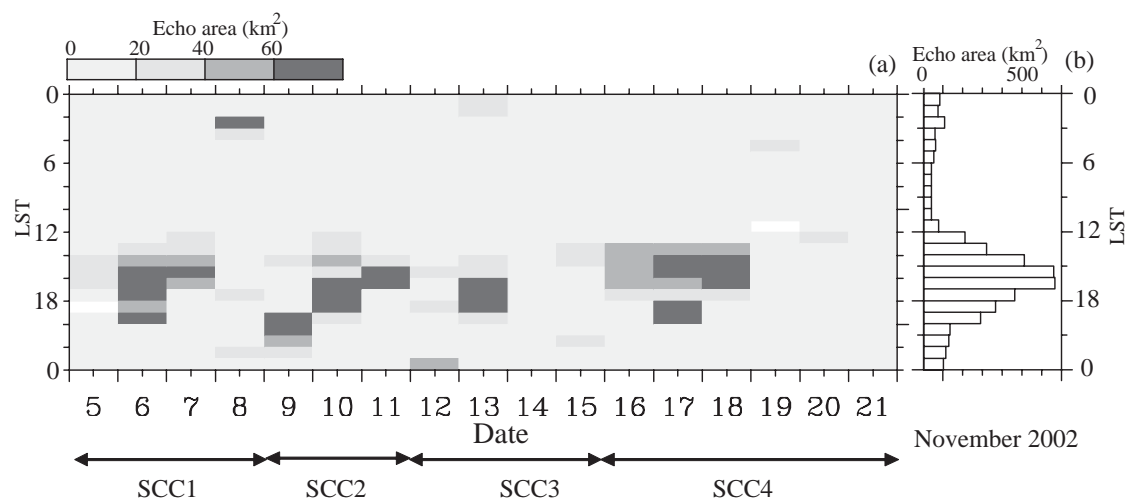
Fig. 11: (a) Local time-day section of intense precipitation echoes ($\geq 40\,\text{dBZ}$) averaged at 1-hour intervals from 05 to 21 November. (b) Diurnal variation of echo area summing up the 1-hour interval data during this analysis period. The echo area is calculated over the whole observational area shown by the circle in Fig. 1b.
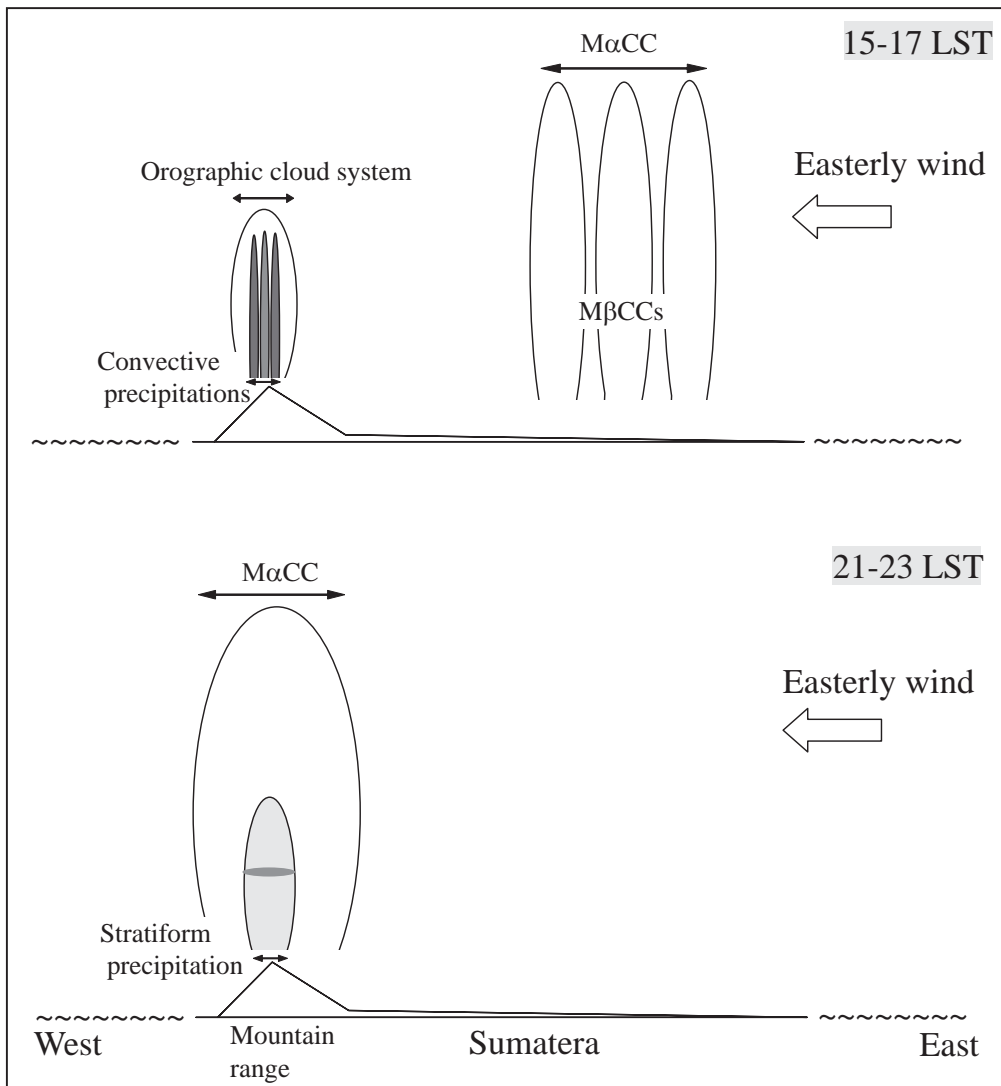
Fig. 12: Schematic illustration of a westward-propagating MαCC over Sumatera and precipitation systems within an orographic cloud system over the mountain region in western Sumatera.